

Spectral time-domain induced polarisation and magnetic surveying – an efficient tool for characterisation of solid waste deposits in developing countries

David Dotse Wemegah^{1,2,*}, Gianluca Fiandaca², Esben Auken², Aboagye Menyeh¹ and Sylvester Kojo Danuor¹

¹*Kwame Nkrumah University of Science and Technology (KNUST), Kumasi, Ghana*

²*Hydrogeophysics Group, Department of Geoscience, Aarhus University, Aarhus, Denmark*

Received April 2015, revision accepted August 2016

ABSTRACT

Time-domain induced polarisation and magnetic data were acquired to map and characterise the decommissioned and un-engineered municipal solid waste disposal site of the Kwame Nkrumah University of Science and Technology, located in the Kumasi Metropolis of Ghana. In this survey, 13 induced polarisation profiles 500–800 m long and 26 magnetic profiles 400–800 m long were acquired. In addition, two boreholes were drilled to help in the interpretation of the geophysical data. The study was carried out with the aim of determining the risk posed by the waste deposit to the quality of the soil and the ground water system, which is the main potable water supply for the Secondary School, the University Teaching Hospital and the Veterinary School, situated within the catchment area of the site. Full-decay 2-D time-domain induced polarisation inversions in terms of Cole–Cole parameters were used for interpreting the induced polarisation data. The chargeability, resistivity and normalised chargeability distributions, together with the magnetic results, aided in a full characterisation of the site geology, the waste and the associated pollution plume. In particular, clear contrasts in resistivity and the polarisation parameters were found between the saprolite layer and the granitic bedrock, which are the main lithological units of the area. Furthermore, it was found that the Kwame Nkrumah University of Science and Technology waste deposit is characterised by a low-chargeability and low-resistivity signature and that the low-resistivity area spreads out from the waste deposit into the permeable saprolite layer, indicating the presence of a leachate plume. A fracture zone in the granitic bedrock beneath the waste deposit, which is a potential conduit for leachate contamination of the ground water system, was also identified. The study thus provides the information needed for assessing the future impact of the waste on the water quality in the area and for designing risk-mitigation actions.

INTRODUCTION

In many parts of the world, municipal solid waste is dumped in landfills (Morris and Barlaz 2011) and, in most cases, without considering its potential effect on the quality of the environment. Although waste management policies have evolved considerably over the last decade (e.g., Butt, Lockley and Oduyemi 2008), many landfills worldwide were (and are still) designed without any kind of capture system underneath, leading to the percolation of leachate through the waste and into the underlying geological layers and aquifer systems (e.g., Christensen *et al.* 1993; Kjeldsen *et al.* 1998a,b; Christensen *et al.* 2001; Poulsen *et al.* 2002).

Landfills without leachate collection systems pose a high risk to the ecosystems and to human health. In the past, this was not

considered much of a problem since large, unused plots of land and abundant natural resources such as water were readily available. However, the ever-increasing population in the urban areas due to rural–urban migration has put pressure on land use, increased waste production, and the demand for potable water without proportionate development in infrastructure to meet the increase in demand especially in developing countries. As well, there are cases of a redefinition of land use. Areas, once considered unsuitable for habitation, such as land used for un-engineered waste disposal, have been inhabited by people, disregarding the risk for public health and livelihood (e.g., Wemegah *et al.* 2014).

The pollutants originating from these un-engineered landfills pose a health risk to the people exposed to them and can lead to death in extreme cases. Effect caused by the intake of pollutants

* ddwemegah.cos@knust.edu.gh

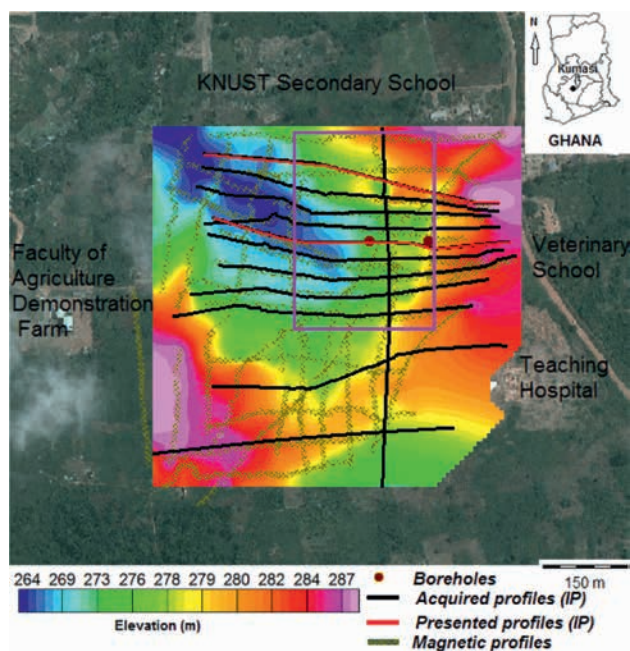


Figure 1 Satellite image of the study area showing the acquired profiles (black and red lines), the borehole positions (dark-red circles), the magnetic lines (dark-green cross), estimated position of waste before research (pink rectangle), and the digital elevation map.

from industry and domestic wastes has been reported by Dolk and Vrijheid (2003), Saunders (2007), and Moore et al. (2011). These pollutants tend to accumulate in the soil and finally leach into the underground water system, which is becoming the main source of potable water supply in most developing countries, due to the ever-increasing pollution of surface water (e.g., Patel, Desai and Desai 2011; Barthiban, Lloyd and Maier 2012) and the drying out of surface water due to climate change. These problems are mostly compounded by improper management of these sites, especially in developing countries like Ghana, because of the lack of capital investment, poor laws and improper enforcement of existing laws.

To improve the situation in some of these areas, there is a need to monitor and determine the impact of the sites on the quality of the environment and to provide the appropriate remedies. For large areas, it is very expensive to obtain information on landfill characterisation using only drillings. Thus, a fast, cheap, reliable, informative, and non-destructive mapping technique, allowing coverage of the whole area of interest, is a huge benefit. Although the mapping of the waste body is a target in itself (for instance, for the recognition and delineation of buried and forgotten landfills), it is also very relevant to identify possible pollution plumes and to assess the geology below the waste, in order to detect potential pollution threats.

In Ghana where waste sorting at the source is not a practice, two geophysical methods are particularly well suited for these purposes, i.e., magnetic surveying and direct current (DC) electrical resistivity imaging with induced polarisation (IP). In this

case, the municipal solid waste contains domestic ferrous materials that produce strong magnetic anomalies that are helpful in delineating the lateral extent of the waste deposit (e.g., Gilkeson, Heigold and Laymon 1986; Barrows and Rocchio 1990; Gibson, Lyle and Gorge 1996; Marchetti et al. 2002; Wemegah et al. 2014). IP has also been used in a variety of environmental applications linked to the characterisation of waste sites, ranging from the detection and mapping of contaminants (e.g., Vanhala 1997; Kemna, Binley and Slater 2004; Sogade et al. 2006; Flores Orozco et al. 2011; Flores Orozco et al. 2012; Johansson, Fiandaca and Dahlin 2014; Wemegah et al. 2014) to geological discrimination (e.g., Schmutz et al. 2010; Gazoty et al. 2012b) and landfill delineation (e.g., Carlson, Hare and Zonge 2001; Leroux, Dahlin and Rosqvist 2010; Gazoty et al. 2012a,b; Wemegah et al. 2014). Furthermore, the time-domain (TD) field IP operation is simple when applying standard multi-channel acquisition systems. New approaches with optimised acquisition parameters (Gazoty et al. 2013) make it possible to get reliable data and to extract the spectral content contained in the TDIP signal. In fact, Fiandaca et al. (2012, 2013) presented two new algorithms for inverting 1-D/2-D TDIP data that use the full-decay IP curves for retrieving the IP spectral information in terms of Cole–Cole parameters (Cole and Cole 1941; Pelton et al. 1978). In terms of the duration of current pulses and stack size, the transmitter waveform is accurately modelled in these inversion algorithms, as well as the effect of low-pass filters that is present in the instruments.

This study presents the characterisation of the (un-engineered and decommissioned) Kwame Nkrumah University of Science and Technology (KNUST) waste disposal site (Kumasi, Ghana) by means of TD spectral IP and magnetic surveying. Thirteen IP profiles 500–800 m long and 26 magnetic profiles 400–800 m long were acquired and two borehole drillings were carried out to provide a priori information to help in the interpretation of the geophysical data. The aim of the investigation is to determine the risk posed by the KNUST landfill on the quality of soil and ground water, which is the main source of water supply to the KNUST Secondary School, the Teaching Hospital and the Veterinary School situated in the area. Furthermore, the risk it poses to the quality of water used for the irrigation of vegetable farms in the catchment area of the waste disposal site which has the potential of affecting the quality of vegetable cultivated in the area and sold to the public.

METHODOLOGY

Study area

The KNUST solid waste disposal site (Figure 1) is situated in the northeastern part of the main KNUST University Campus in the Kumasi Metropolis of the Ashanti Region in southwestern Ghana. It is located around the coordinate (660349W, 739177N) projected in the World Geodetic System (WGS84), Universal Transverse Mercator zone 30N. The area is an un-engineered waste disposal site with no protective layer and leachate collecting system.

It covers an approximate area of 600 m × 650 m with the waste deposited around one-third of the land area. The site was used from 1998 until 2011 when waste disposal in the area was relocated to the Dompoase Landfill, the first engineered waste disposal site constructed in the Kumasi Metropolis. The area is mainly a low-lying wetland (with a topography of less than 274 m in the northwestern area of the site, Figure 1) situated behind the main demonstration farm of the Agriculture Faculty of the university. Other university facilities located in the area are the KNUST Secondary School forming the northern boundary of the site, the KNUST Teaching Hospital and the Veterinary School under construction in the western part of the area. Economically, the people in towns around the site use the area for farming foodstuffs, with the low-lying wetland area in the west (Figure 1) serving as an irrigation farm where vegetables are grown all year round.

The area falls within the semi-equatorial region with two main raining seasons. The major season runs from March to June and the minor season from September to the end of November. The average annual rainfall of the metropolis is between 150 and 170 mm.

Geologically, the metropolis falls within the Kumasi Basin of the Birimian Formation and consists of three main lithological units. These are the thin upper duricrust layer with a thickness in the range of 0.1–0.3 m overlying a 5 to 30 m thick layer of saprolite that averages around 28 m in the university campus and

underlain by a batholithic basin granitoid formerly referred to as the Cape Coast Granitoid. The granitoid is peraluminous, typically granodioritic in composition (K_2O rich) and shows little mineral alteration (Hirdes, Davis and Eisenlohr 1992; Boadi, Wemegah and Preko 2013). The outcrops of this K-feldspar-rich granitic rocks can be seen in most areas of the metropolis (Wright et al. 1985; Kesse 1985; Griffis et al. 2002).

The area has an altitude of 265 m in its northwestern corner with the highest points having an altitude of around 290 m in the eastern part. The drainage mainly follows this pattern and flows northwest in the area.

Waste composition

The materials deposited at the site are mainly domestic wastes from the university halls, departments and the staff's residence. Hospital wastes from the university hospital are also deposited at the site. The waste is mainly composed of organic waste, plastic, bottles, ferrous metal from domestic canned food, papers, and some heavy metals such as lead, manganese from domestic cells, and car batteries. The annual burning of bushes in the area during the dry season has led to the burning of most combustible but non-biodegradable materials such plastics from the area, leaving mainly incombustible materials like glass and metals on the surface of the hip of decayed waste in most parts of the site.

MAGNETIC DATA ACQUISITION AND PROCESSING

The magnetic data were acquired on the site using a Geometrics G856 magnetometer. The data were acquired on approximately 5 m × 15 m grids and on 26 profiles with lengths ranging between 400 and 800 m (Figure 1). The base station for monitoring the diurnal variation of the geomagnetic field for diurnal correction was set at a point of low environmental magnetic influence 1 km from the survey site. The processing of the data was carried out using the Oasis Montaj Software package after the diurnal correction. The gridding of the data was carried out using the minimum curvature algorithm at a quarter of the profile spacing. This algorithm, which is based on splines in tension (Smith and Wessel 1990), substantially increases the smoothness and the lateral consistency of the generated grids (Geosoft Inc. 1995).

To locate the observed magnetic anomalies directly over the magnetic sources since the data were collected at a point of low magnetic latitude, the analytical signal, a form of reduction to the pole (e.g., Nabighian 1984; Roest, Verhoef and Pilkington 1992; MacLeod, Jones and Dai 1993; Li 2008; Ansari and Alamdar 2009), was applied to the total magnetic intensity data. This filter converts data recorded in the inclined Earth's magnetic field to what the data would have looked like if the magnetic field had been vertical (e.g., Geosoft Inc. 1995; Li 2008), thus preventing north–south signals from dominating the data. This gives a representation of the magnetic anomalies, which depends on the location of the magnetic sources and not on the magnetisation direction, thereby aiding in the interpretation (e.g., Debeglia and Corpel 1997).

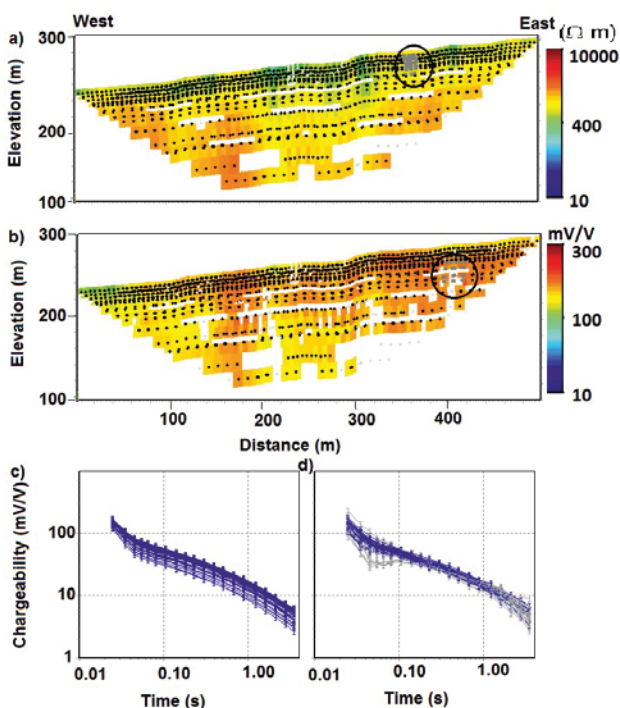


Figure 2 DC and IP data of profile 1: (a) resistivity and (b) chargeability pseudosections of gate 5. (c) Decay curves corresponding to the quadrupoles picked from the black circle on section a. (d) Decay curves (in blue) and deleted outliers (in grey) corresponding to the quadrupoles picked from the black circle on section b.

IP data acquisition and processing

The DCIP survey was performed using the gradient array (Dahlin and Zhou 2006) because of its efficiency with a multi-channel acquisition system, the low geometrical factor, and how it minimises the effect of electrode polarisation (e.g., Dahlin,

Leroux and Nissen 2002; Gazoty *et al.* 2013). The instrument used for the survey was the Iris Syscal Pro instrument. The IP data were acquired using 20 gates, approximately log-sampled with gate widths between 10 and 800 ms and three stacks in each acquisition, using 4-s current turn on and off (Gazoty *et al.* 2013). The electrode spacing used in the survey was 5 m.

All 13 DCIP profiles, including 11 W-E oriented profiles with a length of 500 m each and two crossing profiles with lengths of 800 and 700 m each, were surveyed (Figure 1). The first nine W-E profiles from the north were spaced approximately 50 m from each other, whereas the profile spacing was bigger for the remaining two profiles that were farther away from the waste deposit. Dense vegetation and the marshy nature of the area prevented the obtaining of straight profile lines in some parts of the site.

The data were processed to remove outliers in the resistivity section as well as in the IP decays. Resistivity outliers were identified through the lack of smoothness in the resistivity pseudosection; IP outliers were identified inspecting both the chargeability pseudosections, gate by gate, as well as the IP decays, quadrupole by quadrupole. The resistivity and chargeability (gate 5) pseudosections of profile 1 are shown in Figures 2a,b. Figure 2c presents IP decays without outliers, whereas Figure 2d shows decays with removed outliers. In all, about 5% of the DC data and about 13% of the IP data were removed in the processing. The standard deviation on the DC and IP data was computed using 2% and 10% relative values, respectively, plus a noise floor of 1 mV (Gazoty *et al.* 2013).

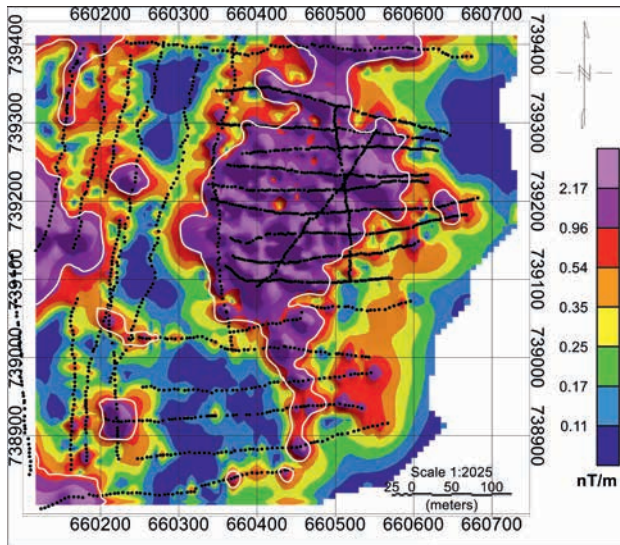


Figure 3 Map of the magnetic analytical signal showing the position of waste with high magnetic signature (bounded by white polylines). Black hollow circles represent the acquisition points.

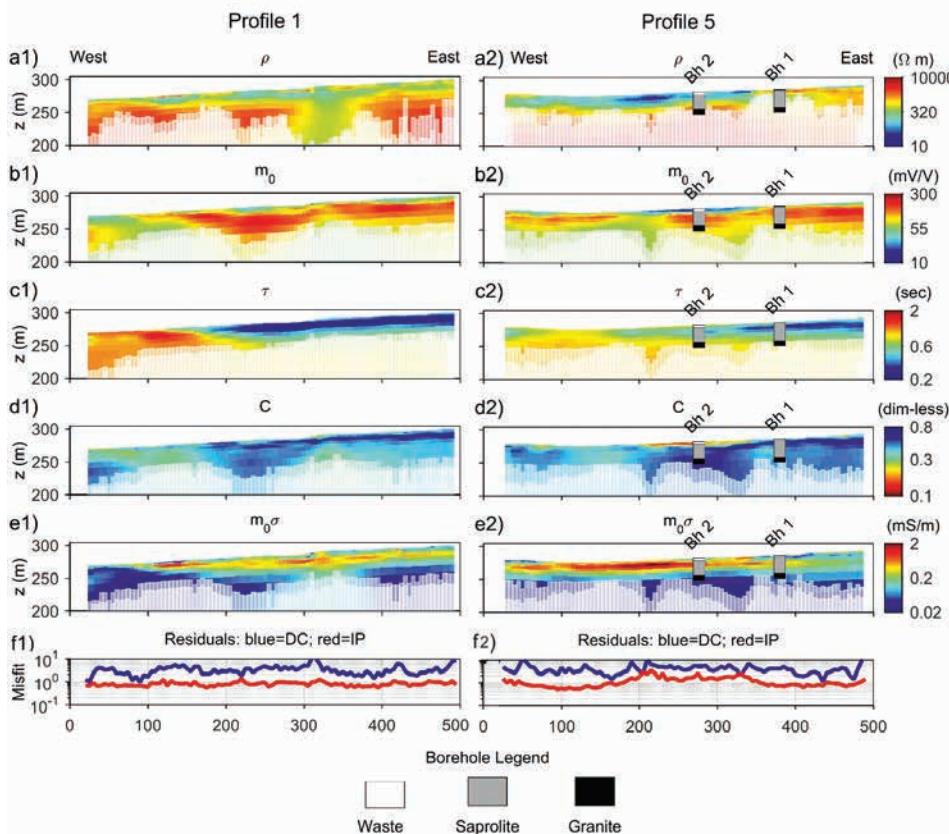


Figure 4 Cole–Cole DCIP parameters of profiles 1 and 5: (a) resistivity section, (b) chargeability section, (c) relaxation time section, (d) frequency factor section, (e) normalised chargeability section, and (f) the DC and the IP misfit section. The DOI is included in all model plots by partially shading poorly resolved areas and fully blanking unresolved model areas.

The acquired DCIP data were inverted in Aarhus Workbench (Auken, Viezzoli and Christiansen 2009), a software package that enables the display, processing, and inversion of the data in a geographic information system environment. To help get *a priori* information to be used as a guide in the interpretation of the geophysical results, two boreholes (one on the main waste body and the other outside the main waste body) were drilled (Figures 1, 4, and 5).

Inversion of DCIP data

The full-decay IP data were inverted using the 2-D DC/IP inversion algorithm (Fiandaca *et al.* 2013; Auken *et al.* 2014). The inversion code takes into account the current waveform and filter characteristic of the instrument (specifically calibrated for the Syscal Pro instrument used in the survey) in the forward computations, allowing for a quantitative interpretation of the IP parameters (Fiandaca *et al.* 2012). This gives access to the spectral information contained in the IP decays, retrieved in terms of the Cole–Cole model (Pelton *et al.* 1978). The inversion Cole–Cole parameters including DC resistivity (ρ), chargeability (m_0), relaxation time (τ), and frequency factor (C) were based on the complex resistivity (ξ) equation:

$$\xi(\omega) = \rho \left[1 - m_0 \left(1 - \frac{1}{1 + (i\omega\tau)^C} \right) \right] \quad (1)$$

where ω is the frequency, and i is the imaginary unit. With the IP time gates adopted in this study, τ values ranging from tens of milliseconds to several seconds can be resolved (Fiandaca *et al.* 2012).

Furthermore, the data misfit is computed along the profiles in

terms of the data residual $\chi = \sqrt{\frac{1}{N} \sum_{i=1}^N \left(\frac{f_i - d_i}{\sigma_i} \right)^2}$, separately for

DC and IP data (d_i , f_i and σ_i represent the i^{th} observed datum, forward computation, and standard deviation, respectively).

RESULTS AND DISCUSSION

The IP and the magnetic datasets acquired in the study were used to develop various models of the study area. These included the delineation of the lateral extent of the waste, as well as the mapping of waste and plume thicknesses. Furthermore, the geological model of the area was developed by depicting the saprolite–granite interface and fracture zones in the granite bedrock.

The magnetic analytical signal of the research area (Figure 3) mapped the waste's lateral extent, due to the high magnetic signature (greater than 0.96 nT/m) of the waste. The main waste was mapped at the central part of the site, with the northern and western parts of the site recording significant anomalous values. This high magnetic signature is attributed to the ferrous metal composition of the waste, mainly from domestic canned food and ferrous medical waste deposited at the site from the university hospital. The uncontrolled nature of the waste deposition at

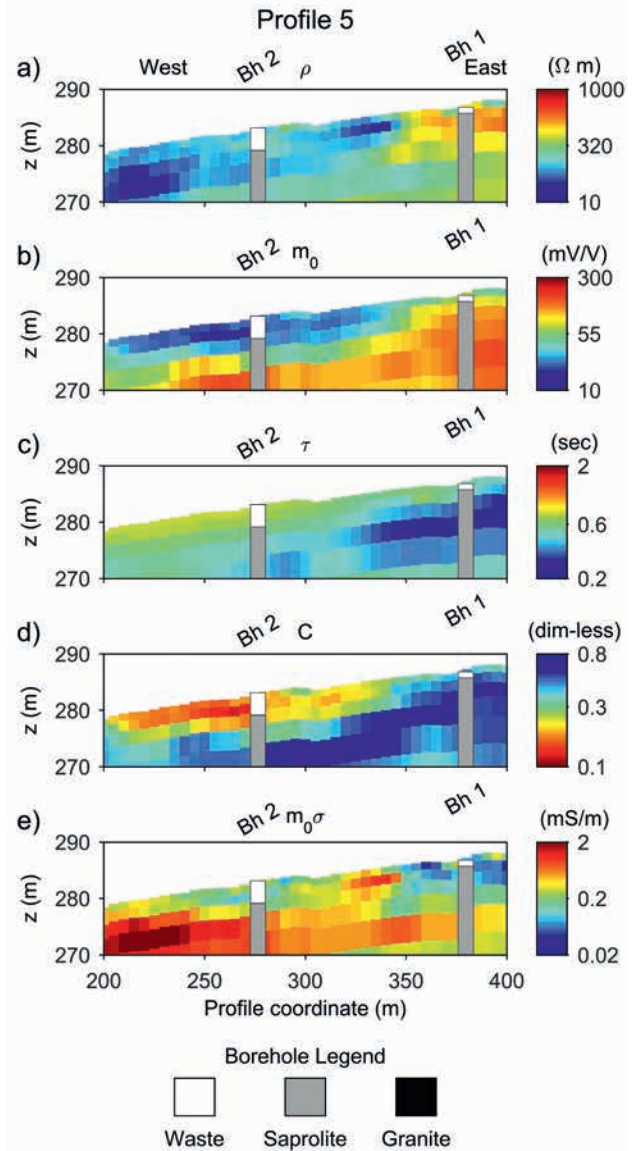


Figure 5 Zoomed-in view of the inversion model of profile 5 presented in Figure 4: (a) resistivity section, (b) chargeability section, (c) relaxation time section, (d) frequency factor section, and (e) normalised chargeability section.

the site is evident in the form of various spots of high magnetic signatures observed in various parts of the area.

The inversion results of two of the TDIP profiles (profile 1 and profile 5 in Figure 1) are presented in Figure 4. A zoomed-in view of profile 5 is shown in Figure 5, for easier comparison of the inversion results with the borehole information at shallow depths. Sections a–d (Figures 4 and 5) represent the Cole–Cole inversion parameters, i.e., resistivity (ρ), chargeability (m_0), relaxation time (τ), and frequency factor (C). Furthermore, the normalised chargeability sections (e), computed as the ratio of the m_0 and ρ parameters, and the misfit sections (f) are presented. Along with the inversion results, the depth of investiga-

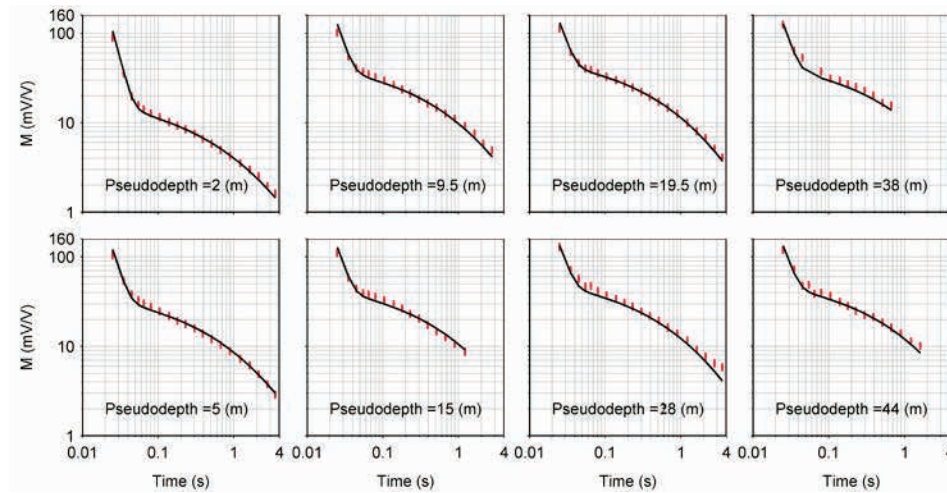


Figure 6 Plot of IP data with error bars (red) and corresponding inversion curves (black) of exemplary decays of profile 5, at different pseudodepths.

tion (DOI) for all inverted parameters is shown in Figures 4 and 5, using the formulation of Fiandaca, Christiansen and Auken (2015). The DOI is included in all model plots by partially shading poorly resolved areas and fully blanking unresolved model areas.

Figure 6 shows fits of the IP decays of profile 5 from various pseudodepths of the IP section. The data are generally well fitted at all depths of the section, with slight deviations at latter times in some decays (pseudodepths 28 and 44 m).

By comparing the borehole logs and the magnetic map in Figure 3 with the TDIP inversions, it is possible to identify several general trends in the distributions of the Cole–Cole parameters, in the presented profiles in Figures 4 and 5 as well as in the other profiles in Figure 1.

- A significant contrast is present between saprolite and granite in terms of resistivity (ρ), chargeability (m_0), and relaxation time (τ). In particular, (i) the granite resistivity is at least 50 times higher than saprolite resistivity, except in localised areas where the granite resistivity decreases significantly; (ii) the saprolite chargeability (m_0) is about one order of magnitude higher than the granite chargeability, except in areas of low resistivity where the contrast is smaller or absent (e.g., Figure 4b2, around 200 m along the profile); and (iii) the relaxation time (τ) is smaller in the saprolite layer.
- In the saprolite layer, a spatial correlation between low-resistivity and low-chargeability areas is present (e.g., Figure 4b2, around 200 m along the profile). The normalised chargeability (σm_0) sections show smaller lateral variability when compared with the resistivity (ρ) and chargeability (m_0) sections, and the σm_0 vertical contrast between saprolite and granite layers is higher than both the resistivity and chargeability contrasts.
- The lateral extent of the waste as mapped from the magnetic data and the waste thickness measured in the borehole logs correlate with areas of low m_0 and C values and slightly high τ values (e.g., Figures 5b–d).
- The resistivity values in the vicinity of the waste areas in the saprolite layer are significantly smaller than in the zones far

from the waste, but the areas of decreased resistivity are larger than the waste extent, both vertically (e.g., Figure 5a) and horizontally (e.g., Figure 4a2).

- Localised areas of low resistivity are present in the granite layer, with more than two orders of magnitude of resistivity contrast (e.g., Figure 4a1, from 300 to 360 m along the profile). These signature areas are spatially observed and correlated in adjacent profiles.

The high chargeability (m_0) values of the saprolite layer can be explained by the presence of haematite in the saprolite composition, as evidenced by the x-ray diffraction analysis that was carried out on soil samples recovered from the drillings.

The decreased resistivity values in the vicinity of the waste body, as retrieved by the IP parameters together with the correlation of low-resistivity and low-chargeability values in the saprolite layer, are probably due to an increase in the pore fluid conductivity of the leachate. In fact, as documented by Lesmes and Frye (2001) and Slater and Lesmes (2002), an increase in fluid conductivity would imply a reduction in both the resistivity and chargeability values. Consequently, the low-resistivity areas can be interpreted as areas polluted by the waste leachate. This interpretation is also corroborated by the thickness of the low-resistivity anomalies, which is significantly bigger than the waste thickness, as known from waste site records and confirmed by the borehole loggings (e.g., Figure 5a). This means that the DC resistivity method alone is not enough for mapping the waste body in this unprotected and un-engineered waste site, where the leachate infiltrates from the waste into the porous subsoil. This interpretation of the low-resistivity anomalies suggests that the normalised chargeability is the better parameter linked to the site lithology. In fact, both chargeability (m_0) and resistivity (ρ) decrease when the pore fluid conductivity increases, but their ratio, i.e., the normalised chargeability σm_0 , is less affected by the pore fluid conductivity.

The localised areas of low resistivity present in the granite bedrock were interpreted as fracture zones. The Birimian sedi-

ment basin, which consists of the weathered zone of the saprolite top layer, has various associated fracture zones within the granitic bedrock, often containing mylonites, which serve as a potential aquifer (Wright et al. 1985; Wright and Burgess 1992). Kortatsi (1994) stated that the fracture zone aquifers normally occur at some depth beneath the weathered zone. These zones, which are mostly water saturated, produce a low-resistivity signature as observed in Figure 4a1. This signature was also observed in the adjacent profiles and was therefore attributed to the presence of fracture zones in the study area.

Contrary to the resistivity distribution, two IP parameters show a signature clearly linked to the waste body. In fact, the waste shows low m_0 and C values, typically below 50 mV/V and 0.2, respectively, smaller than the saprolite values. This is different from what is usually reported in the literature, where, generally, the waste presents high chargeability values (e.g., Slater and Lesmes 2002; Gazoty et al. 2012a,b; Gazoty et al. 2013). However, the low-chargeability signature of the waste body in comparison to the saprolite layer is a clear data-driven feature, because lower IP values at shallow depths are present in the chargeability pseudosections in correspondence with the waste body. Furthermore, there is a good agreement between the low m_0 and C anomalies in Figure 5 and the waste thickness measured in the boreholes. The low-chargeability signature of the waste body is probably due to the waste composition and the annual burning of the area, which leads to decreased biological activity in the waste.

The distinct signatures in the Cole–Cole IP parameters associated with the various features of interest make it possible for the development of their associated models. Consequently, the chargeability, resistivity, and normalised chargeability results were used to map the waste, leachate plume, and the saprolite–granite interface, as shown in Figure 7 for profiles 1 and 5. In particular, profile 1 (Figures 7a1–c1) is on the edge of the site and shows a distinct reduction in resistivity in the granite bedrock interpreted as a fracture zone, and profile 5 (Figures 7a2–

c2) is over the main waste and presents anomalies linked to the waste itself and the resulting pollution plume. Interface picking was performed with the ad hoc tool provided in Aarhus Workbench (Auken, Viezzoli, and Christiansen 2009). Mapping was carried out by picking the elevations of the bottom interface of (i) the low m_0 anomaly (below 50 mV/V) in the chargeability sections (waste bottom), (ii) the low-resistivity anomaly (below 140 Ω m) in the resistivity sections (plume depth extent), and (iii) the anomaly (greater than 0.09 mS/m) in the normalised chargeability sections (the saprolite–granite interface). The example of the picked interfaces (profiles 1 and 5) that were used to generate the waste thickness and plume thickness and the geological models of the study area are also shown in Figure 7, together with the two boreholes drilled in the study area, showing waste thicknesses and geological logs.

The elevation values of the respective interfaces from all the surveyed profiles were then gridded using the ordinary kriging algorithm to generate the waste bottom, plume bottom, and saprolite bottom (saprolite–granite interface) surfaces. Furthermore, the thickness models of the features were obtained by subtracting the gridded surfaces from the digital elevation model of the area.

Figure 8 presents the mapped waste thickness delineated using the low-chargeability signature from the IP inversion models. From the result, the main waste was mapped in the central position of the site with thickness ranging from 3 to 10 m. The waste mapped in the western boundary of the site is the area where the waste was spread from the main disposal site. The waste mapped at the northern part of the site extends into the KNUST Secondary School compound. Superimposed on the waste thickness map is an isoline (blacklines, Figure 8) of the high magnetic analytical signal (1 nT/m) of the magnetic data for easy comparison with the two results. The lateral extent of the mapped waste, mapped from the IP data, is in agreement with the magnetic results (magnetic analytical signal isoline in Figures 3 and 8), but with a smaller extension. The smaller lateral extension of the waste mapped by IP is probably due to the different

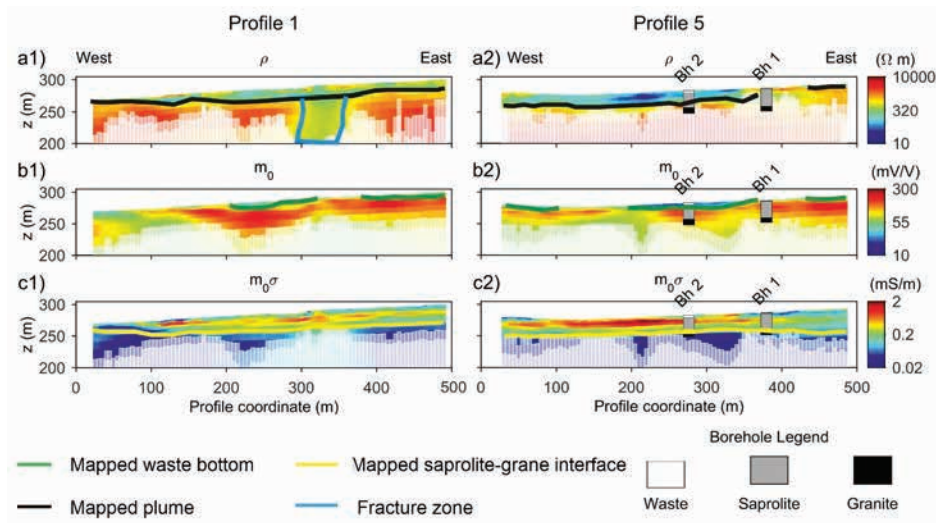


Figure 7 Cole–Cole DCIP parameters of profiles 1 and 5 showing picked interfaces used in developing plume, waste thickness, and lithological models: (a) resistivity section showing the picked plume bottom and fracture zone, (b) chargeability section showing the picked waste bottom, and (c) normalised chargeability section showing the picked saprolite–granite interface.

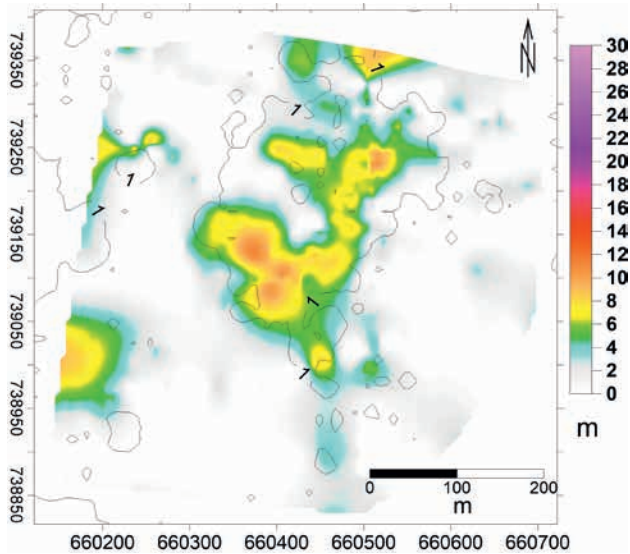


Figure 8 Delineated waste thickness mapped from chargeability sections, with superimposed isolines of analytical signal (Figure 3) at 1 nT/m (black lines).

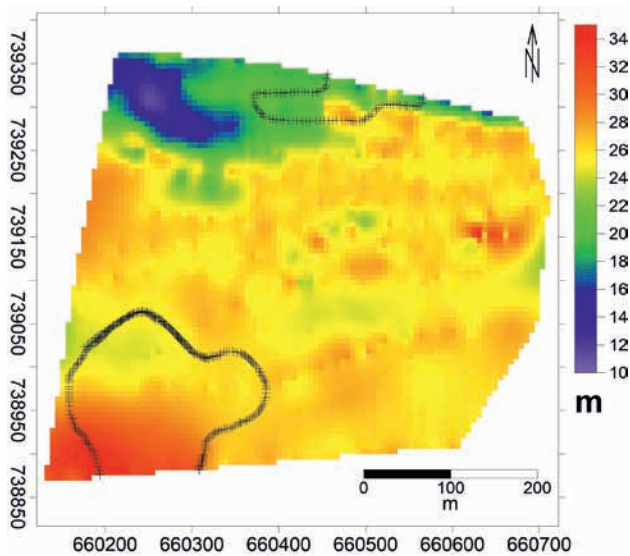


Figure 9 Mapped saprolite thickness with superimposed mapped fracture zones in the granitic bedrock (black lines).

sensitivity levels of the two methods to thin waste layers: the IP inversions cannot resolve a waste thickness significantly smaller than the electrode spacing.

Figure 9 shows the saprolite thickness derived from the normalised chargeability sections. The thickness of the saprolite is quite homogeneous in the surveyed area, with values around 26 m, except in the northwestern part of the site, where it thins to about 10 m, and in the southwestern part, where it reaches values greater than 30 m. The thinner area corresponds to the zone of low elevation (Figure 1) carrying the river channel. In Figure 9, two fracture zones, gathered from the low-resistivity anomalies in the granite bedrocks, are also shown.

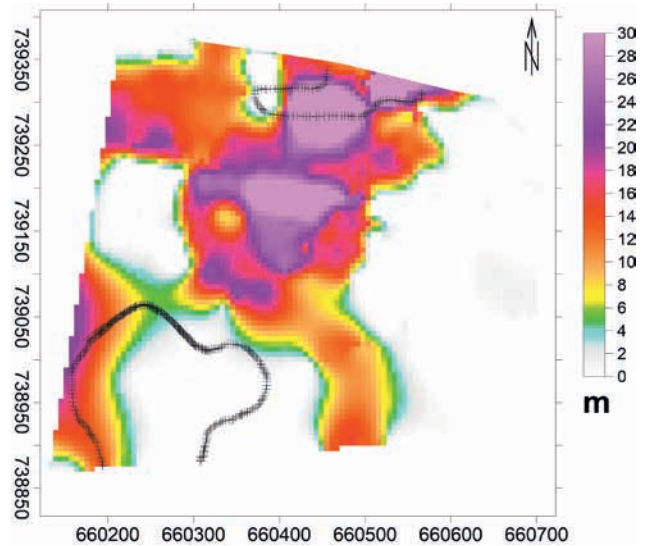


Figure 10 Plume thickness map with superimposed mapped fracture zones in the granitic bedrock (black lines).

Finally, Figure 10 presents the map of the plume thickness. The plume shows a bigger lateral and vertical extension than the waste body, as is clear by comparing the waste thickness map in Figure 8 (the same thickness colour scale has been used in Figures 8 and 10 for easier comparison). The greatest plume thicknesses (>20 m) were mapped below the main waste (Figures 3 and 8). Note the wide plume in the low-lying area in the northwestern section of the site. We attribute this to leachate flow through the river channel.

The superimposed fracture zones on the plume map provide an insight into the vulnerability of the ground water system to waste contamination. The fracture zones in the impermeable granitic bedrock serve as the means for ground water recharge, hence a potential conduit for leachate when connected. The fracture zone in the northern part of the site is beneath the waste body, in an area of deep leachate infiltration (Figures 8 and 10). This poses a high risk for ground water contamination and endangers the quality of the water supply to the secondary school, the veterinary school, and the hospital.

CONCLUSION

Combined 2-D TD spectral IP tomography and magnetic surveying were used in mapping the un-engineered municipal solid waste deposit of the KNUST, located in the Kumasi Metropolis of Ghana. The full-decay IP data were inverted using an accurate modelling of the current waveform and of the instrument filter to extract the IP spectral information in terms of Cole–Cole parameters, while the analytical signal image was computed from the magnetic data.

The image produced from the magnetic data depicted the lateral extent of the landfill, due to its high magnetic signature, whereas the IP investigation retrieved the thickness of the waste body, together with information on the waste leachate and on the site geology. In particular, it was found that the waste deposit is

characterised by a low-chargeability and low-resistivity signature and that the low-resistivity area spreads out from the waste deposit into the permeable saprolite layer, indicating the presence of a leachate plume. Furthermore, a lithological setup of the site was developed, due to the contrast present in both resistivity and IP parameters between the saprolite layer and the granite bedrock, which are the main lithological units of the area. A fracture zone within the granite bedrock was identified, which may increase the risk of leachate contaminating the underlying ground water aquifer.

The outcome of this work is important for planning the future provision of potable water to the institutions located in the area, since ground water has become the main means of water supply on a regular basis in the Kumasi Metropolis in recent years. This is due to the erratic supply of water from the Ghana Water and Sewage Company, which has the potential to endanger the safe running of the facility.

We believe that the full-decay spectral inversion of TDIP data could contribute towards changing the field applications of IP. Data interpretation could evolve from a qualitative description of the soil, able only to discriminate the presence of contrasts in chargeability parameters, towards a quantitative analysis of the investigated media, which could allow soil-type characterisation, as done in this study. We also believe that the combination of TDIP and magnetic surveying is a strong and efficient tool for the mapping of waste deposits and the host geology in developing countries.

ACKNOWLEDGEMENTS

The authors would like to thank the DANIDA Fellowship Centre and the Kwame Nkrumah University of Science and Technology for supporting this research on the Building Stronger University, Environment and Climate Platform.

REFERENCES

- Ansari A.H. and Alamdar K. 2009. Reduction to the pole of magnetic anomalies using analytic signal. *World Applied Sciences Journal* **7**(4), 405–409.
- Auken E., Viezzoli A. and Christiansen A.V. 2009. A single software for processing, inverting, and presentation of AEM data of different systems: the Aarhus Workbench. Australian Society of Exploration Geophysicists (ASEG) 2009, Sydney, Australia, Expanded Abstracts, 1–5.
- Auken E., Christiansen A.V., Kirkegaard C., Fiandaca G., Schamper C., Behroozmand A.A. *et al.* 2014. An overview of a highly versatile forward and stable inverse algorithm for airborne, ground-based and borehole electromagnetic and electric data. *Exploration Geophysics*, A–M.
- Barrows L. and Rocchio J.E. 1990. Magnetic surveying for buried metallic objects. *Groundwater Monitoring and Remediation* **10**(3), 204–211.
- Barthiban S., Lloyd B.J. and Maier M. 2012. Microbial quality of open dug wells in the Maldives Islands. *Journal of Water Resource and Protection* **4**, 474–486.
- Boadi B., Wemegah D.D. and Preko K. 2013. Geological and structural interpretation of the Konongo Area of the Ashanti Gold Belt of Ghana from aeromagnetic and radiometric data. *International Research Journal of Geology and Mining* **3**(3), 124–135.
- Butt T.E., Lockley E. and Oduyemi K.O.K. 2008. Risk assessment of landfill disposal sites—state of the art. *Waste Management* **28**, 952–964.
- Carlson N.R., Hare J.L. and Zonge K.L. 2001. Buried landfill delineation with induced polarization: progress and problems. *Proceedings of the 2001 Symposium on the Application of Geophysics to Engineering and Environmental Problems*, Denver, CO, March 4–7, 2001.
- Christensen T.H., Kjeldsen P., Albrechtsen H.-J., Heron G., Nielsen P.H., Bjerg P.L. *et al.* 1993. Attenuation of landfill leachate pollutants in aquifers. *Critical Reviews in Environmental Science and Technology* **24**, 119–202.
- Christensen T.H., Kjeldsen P., Bjerg P.L., Jensen D.L., Christensen J.B. and Baun A. 2001. Review: Biogeochemistry of landfill leachate plumes. *Applied Geochemistry* **16**, 659–718.
- Cole K.S. and Cole R.H. 1941. Dispersion and absorption in dielectrics. *Journal of Chemical Physics* **9**, 341–351.
- Dahlin T., Leroux V. and Nissen J. 2002. Measuring techniques in induced polarisation imaging. *Journal of Applied Geophysics* **50**, 279–298.
- Dahlin T. and Zhou B. 2006. Multiple-gradient array measurements for multi-channel 2D resistivity imaging. *Near Surface Geophysics* **4**, 113–123.
- Debeglia N. and Coppel J. 1997. Automatic 3-D interpretation of potential field data using analytic signal derivatives. *Geophysics* **62**, 87–96.
- Dolk H. and Vrijheid M. 2003. The impact of environmental pollution on congenital anomalies. *British Medical Bulletin* **68**, 25–45.
- Fiandaca G., Auken E., Christiansen A.V. and Gazoty A. 2012. Time-domain-induced polarization: full-decay forward modeling and 1-D laterally constrained inversion of Cole–Cole parameters. *Geophysics* **77**(33), E213–E225.
- Fiandaca G., Ramm J., Binley A., Gazoty A., Christiansen A.V. and Auken E. 2013. Resolving spectral information from time domain induced polarization data through 2-D inversion. *Geophysics Journal International* **192**, 631–646.
- Fiandaca G., Christiansen A.V. and Auken E. 2015. Depth of investigation for multi-parameters inversions. *Near Surface Geoscience 2015*, Torino, Italy, Extended Abstracts.
- Flores Orozco A., Williams K.H., Long P.E., Hubbard S.S. and Kemna A. 2011. Using complex resistivity imaging to infer biogeochemical processes associated with bioremediation of a uranium-contaminated aquifer. *Journal of Geophysical Research G: Biogeosciences* **116**(3), G03001.
- Flores Orozco A., Kemna A., Oberdörster C., Zschornack L., Leven C., Dietrich P. *et al.* 2012. Delineation of subsurface hydrocarbon contamination at a former hydrogenation plant using spectral induced polarization imaging. *Journal of Contaminant Hydrology* **136**(137), 131–144.
- Gazoty A., Fiandaca G., Pedersen E., Auken E. and Christiansen A.V. 2012a. Mapping of landfills using time-domain spectral induced polarization data: the Eskelund case study. *Near Surface Geophysics* **10**, 575–586.
- Gazoty A., Fiandaca G., Pedersen E., Auken E., Christiansen A.V. and Pedersen J.K. 2012b. Application of time domain induced polarization to the mapping of lithotypes in a landfill site. *Hydrology and Earth System Sciences* **16**, 1793–1804.
- Gazoty A., Fiandaca G., Pedersen J., Auken E. and Christiansen A.V. 2013. Data repeatability and acquisition techniques for time-domain spectral induced polarization. *Near Surface Geophysics* **11**, 391–406.
- Geosoft Inc. 1995. OASIS Airborne Radiometric Processing System Version 1.0 User's Guide, Geosoft Incorporated, Toronto.
- Gibson P.J., Lyle P. and Gorge D.M. 1996. Environmental applications of magnetometry profiling. *Environmental Geology* **27**, 178–183.

- Gilkeson R.H., Heigold P.C. and Laymon D.E. 1986. Practical application of theoretical models to magnetometer surveys on hazardous waste disposal sites—a case history. *Ground Water Monitoring Review* **6**(1), 54–61.
- Griffis R.J., Barning K., Agezo F.L. and Akosah F.K. 2002. Gold Deposits of Ghana. Minerals Commission Report, 19–37, 163–169.
- Hirdes W., Davis D.W. and Eisenlohr B.N. 1992. Reassessment of Proterozoic granitoid ages in Ghana on the basis of U/Pb zircon and monazite dating. *Precambrian Research* **56**, 89–96.
- Johansson S., Fiandaca G. and Dahlin T. 2014. Field application of resistivity and spectral time domain IP to investigate geoelectrical signatures of free-phase PCE. Near Surface Geoscience 2014, Athens, Greece, Extended Abstracts.
- Kemna A., Binley A. and Slater L. 2004. Crosshole IP imaging for engineering and environmental applications. *Geophysics* **69**, 97–107.
- Kesse G.O. 1985. *The Mineral and Rock Resources of Ghana*, 610. Rotterdam: A.A. Balkema.
- Kjeldsen P., Bjerg P.L., Rügge K., Christensen T.H. and Pedersen J.K. 1998a. Characterization of an old municipal landfill (Grinsted, Denmark) as a groundwater pollution source: landfill hydrology and leachate migration. *Waste Management & Research* **16**(1), 14–22.
- Kjeldsen P., Grundtvig A., Winther P. and Andersen J.S. 1998b. Characterization of an old municipal landfill (Grinsted, Denmark) as a groundwater pollution source: landfill history and leachate composition. *Waste Management & Research* **16**(1), 3–13.
- Kortatsi B.K. 1994. Groundwater utilization in Ghana. In: *IAHS Publications* 222, 151. Accra, Ghana: Water Resources Research Institute.
- Leroux V., Dahlin T. and Rosqvist H. 2010. Time-domain IP and resistivity sections measured at four landfills with different contents. Near Surface 2010, Zürich, Switzerland, Expanded Abstracts, P09.
- Lesmes D.P. and Frye K.M. 2001. Influence in pore fluid chemistry on the complex conductivity and induced polarization responses of Berea sandstone. *Journal of Geophysical Research* **106**, 4079–4090.
- Li X. 2008. Magnetic reduction-to-the-pole at low latitudes: observations and considerations. *Lead. Edge* **27**, 990–1002.
- MacLeod I.N., Jones K. and Dai T.F. 1993. 3-D analytic signal in the interpretation of total magnetic field data at low magnetic latitudes. *Exploration Geophysics* **24**, 679–688.
- Marchetti M., Cafarella L., Di Mauro D. and Zirizzotti A. 2002. Ground magnetometric surveys and integrated geophysical methods for solid buried waste detection: a case study. *Annals of Geophysics* **45**(3/4), 563–573.
- Moore E., Matalon E., Clary J., Firestone L. and Anda S.D. 2011. *The Human Costs of Nitrate-Contaminated Drinking Water in the San Joaquin Valley*, 1st edn. Oakland, CA: Pacific Institute for Studies in Development, 45.
- Morris J.W.F. and Barlaz M.A. 2011. A performance-based system for the long-term management of municipal waste landfills. *Waste Management* **31**, 649–662.
- Nabighian M.N. 1984. Toward a three-dimensional automatic interpretation of potential field data via generalised Hilbert transforms: fundamental relations. *Geophysics* **49**, 780–789.
- Patel P., Desai M. and Desai J. 2011. Geotechnical parameters impact on artificial ground water recharging technique for Urban Centers. *Journal of Water Resource and Protection* **3**, 275–282.
- Pelton W.H., Ward S.H., Halof P.G., Sill W.R. and Nelson P.H. 1978. Mineral discrimination and removal of inductive coupling with multi-frequency induced polarization. *Geophysics* **43**, 588–609.
- Poulsen T.G., Moldrup P., Sørensen K. and Hansen J.A. 2002. Linking landfill hydrology and leachate chemical composition at a controlled municipal landfill (Kåstrup, Denmark) using state-space analysis. *Waste Management & Research* **20**, 445–456.
- Roest W.R., Verhoef J. and Pilkington M. 1992. Magnetic interpretation using the 3-D analytical signal. *Geophysics* **57**, 116–125.
- Saunders P. 2007. A systematic review of the evidence of an increased risk of adverse birth outcomes in populations living in the vicinity of landfill waste disposal sites. In: *Population Health and Waste Management: Scientific Data and Policy Options. Report of a WHO Workshop Rome, Italy, 29–30 March 2007* (eds F. Mitis and M. Martuzzi), 25–27. Copenhagen, Denmark: WHO Regional Office for Europe.
- Schmutz M., Revil A., Vaudelet P., Batzle M., Viñao P.F. and Werkema D.D. 2010. Influence of oil saturation upon spectral induced polarization of oil-bearing sands. *Geophysical Journal International* **183**, 211–224.
- Slater L.D. and Lesmes D.P. 2002. IP interpretation in environmental investigations. *Geophysics* **67**, 77–88.
- Smith W.H.F. and Wessel P. 1990. Gridding with continuous curvature splines in tension. *Geophysics* **55**(3), 293–305.
- Sogade J.A., Scira-Scappuzzo F., Vichabian Y., Shi W., Rodi W., Lesmes D.P. et al. 2006. Induced-polarization detection and mapping of contaminant plumes. *Geophysics* **71**, B75–B84.
- Vanhala H. 1997. Mapping oil-contaminated sand and till with the spectral induced polarization (SIP) method. *Geophysical Prospecting* **45**, 303–326.
- Wemegah D.D., Fiandaca G., Auken E., Menyeh A. and Danuor S.K. 2014. Spectral time-domain IP and magnetic for mapping municipal solid waste deposits in Ghana. 20th European Meeting of Environmental and Engineering Geophysics, Athens, Greece, 14–18 September 2014, Extend Abstracts.
- Wright J.B., Hastings D.A., Jones W.B. and Williams H.R. 1985. *Geology and Mineral Resources of West Africa*, 165. London: Allen & Unwin.
- Wright E.P. and Burgess W.G. (eds) 1992. The hydrogeology of crystalline basement aquifers in Africa. *Geological Society Special Publication* **66**, 1–27.